Cascaded modulator architecture for WDM applications

Kapil Debnath,[1] Liam O'Faolain,[1,4,*] Frederic Y. Gardes,[2] Andreas G. Steffan,[3] Graham T. Reed,[2] and Thomas F. Krauss[1]

[1]*School of Physics & Astronomy, University of St Andrews, North Haugh, St Andrews KY16 9SS, UK*
[2]*Optoelectronics Research Centre, University of Southampton, Southampton, SO17 1BJ, UK*
[3]*u²t Photonics AG, Berlin, Reuchlinstrasse 10-11, 10533 Berlin, Germany*
[4]*Ginzton Laboratory, Stanford University, 450 Via Pueblo Mall, Stanford, California 94305-4088, USA*
[*]*jww1@st-andrews.ac.uk*

Abstract: Integration density, channel scalability, low switching energy and low insertion loss are the major prerequisites for on-chip WDM systems. A number of device geometries have already been demonstrated that fulfill these criteria, at least in part, but combining all of the requirements is still a difficult challenge. Here, we propose and demonstrate a novel architecture consisting of an array of photonic crystal modulators connected by a dielectric bus waveguide. The device architecture features very high scalability and the modulators operate with an AC energy consumption of less than 1fJ/bit. Furthermore, we demonstrate cascadeability and multichannel operation by using a comb laser as the source that simultaneously drives 5 channels.

OCIS codes: (350.4238) Nanophotonics and photonic crystals; (230.2090) Electro-optical devices; (130.3120) Integrated optics devices; (250.5300) Photonic integrated circuits.

References and links

1. Q. Xu, B. Schmidt, J. Shakya, and M. Lipson, "Cascaded silicon micro-ring modulators for WDM optical interconnection," Opt. Express **14**(20), 9431–9435 (2006).
2. L. Chen, C. R. Doerr, P. Dong, and Y.-K. Chen, "Monolithic silicon chip with 10 modulator channels at 25 Gbps and 100-GHz spacing," Opt. Express **19**(26), B946–B951 (2011).
3. S. Ren, Y. Rong, S. A. Claussen, R. K. Schaevitz, T. I. Kamins, J. S. Harris, and D. A. B. Miller, "Ge/SiGe quantum well waveguide modulator monolithically integrated with SOI waveguides," IEEE Photon. Technol. Lett. **24**(6), 461–463 (2012).
4. M. Notomi, "Manipulating light with strongly modulated photonic crystals," Rep. Prog. Phys. **73**(9), 096501 (2010).
5. B.-S. Song, S. Noda, T. Asano, and Y. Akahane, "Ultra-high-Q photonic double-heterostructure nanocavity," Nat. Mater. **4**(3), 207–210 (2005).
6. E. Kuramochi, M. Notomi, S. Mitsugi, A. Shinya, T. Tanabe, and T. Watanabe, "Ultrahigh-Q photonic crystal nanocavities realized by the local width modulation of a line defect," Appl. Phys. Lett. **88**(4), 041112 (2006).
7. K. Welna, S. L. Portalupi, M. Galli, L. O'Faolain, and T. F. Krauss, "Novel Dispersion Adapted Photonic Crystal Cavity with Improved Disorder Stability," IEEE J. Quantum Electron. **48**(9), 1177–1183 (2012).
8. B.-S. Song, T. Nagashima, T. Asano, and S. Noda, "Resonant-wavelength control of nanocavities by nanometer-scaled adjustment of two-dimensional photonic crystal slab structures," IEEE Photon. Technol. Lett. **20**(7), 532–534 (2008).
9. T. Tanabe, K. Nishiguchi, E. Kuramochi, and M. Notomi, "Low power and fast electro-optic silicon modulator with lateral p-i-n embedded photonic crystal nanocavity," Opt. Express **17**(25), 22505–22513 (2009).
10. R. G. Beausoleil, J. Ahn, N. Binkert, A. Davis, D. Fattal, M. Fiorentino, N. P. Jouppi, M. McLaren, C. M. Santori, R. S. Schreiber, S. M. Spillane, D. Vantrease, and Q. Xu, "A nanophotonic interconnect for high-performance many-core computation," 16th IEEE Symposium on High Performance Interconnects, 182–189 (2008).
11. A. Kovsh, A. Gubenko, I. Krestnikov, D. Livshits, S. Mikhrin, J. Weimert, L. West, G. Wojcik, D. Yin, C. Bornholdt, N. Grote, M. V. Maximov, and A. Zhukov, "Quantum dot comb-laser as efficient light source for silicon photonics," Proc. Soc. Photo Opt. Instrum. Eng. **7230**, 72300M (2009).
12. D. Miller, "Device requirements for optical interconnects to silicon chips," Proc. IEEE **97**(7), 1166–1185 (2009).
13. L. Chen, C. R. Doerr, Y.-K. Chen, and T.-Y. Liow, "Low-loss and broadband cantilever couplers between standard cleaved fibers and high-index-contrast Si_3N_4 or Si waveguides," IEEE Photon. Technol. Lett. **22**(23), 1744–1746 (2010).

#176485 - $15.00 USD Received 18 Sep 2012; revised 10 Nov 2012; accepted 14 Nov 2012; published 26 Nov 2012

14. M. Grande, L. O'Faolain, T. P. White, M. Spurny, A. D'Orazio, and T. F. Krauss, "Optical filter with very large stopband (approximately 300 nm) based on a photonic-crystal vertical-directional coupler," Opt. Lett. **34**(21), 3292–3294 (2009).
15. F. Morichetti, A. Melloni, M. Martinelli, R. G. Heideman, A. Leinse, D. H. Geuzebroek, and A. Borreman, "Box-shaped dielectric waveguides: a new concept in integrated optics," J. Lightwave Technol. **25**(9), 2579–2589 (2007).
16. P. Cardile, G. Franzò, R. Lo Savio, M. Galli, T. F. Krauss, F. Priolo, and L. O' Faolain, "Electrical conduction and optical properties of doped silicon-on-insulator photonic crystals," Appl. Phys. Lett. **98**(20), 203506 (2011).
17. C. P. Reardon, I. H. Rey, K. Welna, L. O'Faolain, and T. F. Krauss, "Fabrication and characterisation of both photonic crystal slow light waveguides and cavities," J. Vis. Exp. in press.
18. T. P. White, L. O'Faolain, J. Li, L. C. Andreani, and T. F. Krauss, "Silica-embedded silicon photonic crystal waveguides," Opt. Express **16**(21), 17076–17081 (2008).
19. J. F. Buckwalter, X. Zheng, G. Li, K. Raj, and A. V. Krishnamoorthy, "A monolithic 25-Gb/s transceiver with photonic ring modulators and Ge detectors in a 130-nm CMOS SOI process," IEEE J. Solid-state Circuits **47**(6), 1309–1322 (2012).
20. S. L. Portalupi, M. Galli, M. Belotti, L. C. Andreani, T. F. Krauss, and L. O'Faolain, "Deliberate versus intrinsic disorder in photonic crystal nanocavities investigated by resonant light scattering," Phys. Rev. B **84**(4), 045423 (2011).
21. C. J. Chen, J. Zheng, T. Gu, J. F. McMillan, M. Yu, G.-Q. Lo, D.-L. Kwong, and C. W. Wong, "Selective tuning of high-Q silicon photonic crystal nanocavities via laser-assisted local oxidation," Opt. Express **19**(13), 12480–12489 (2011).
22. P. Dong, W. Qian, H. Liang, R. Shafiiha, N.-N. Feng, D. Feng, X. Zheng, A. V. Krishnamoorthy, and M. Asghari, "Low power and compact reconfigurable multiplexing devices based on silicon microring resonators," Opt. Express **18**(10), 9852–9858 (2010).
23. L. Chen, K. Preston, S. Manipatruni, and M. Lipson, "Integrated GHz silicon photonic interconnect with micrometer-scale modulators and detectors," Opt. Express **17**(17), 15248–15256 (2009).
24. D. J. Thomson, F. Y. Gardes, J.-M. Fedeli, S. Zlatanovic, Y. Hu, B. P. P. Kuo, E. Myslivets, N. Alic, S. Radic, G. Z. Mashanovich, and G. T. Reed, "50-Gb/s silicon optical modulator," IEEE Photon. Technol. Lett. **24**(4), 234–236 (2012).
25. H. C. Nguyen, Y. Sakai, M. Shinkawa, N. Ishikura, and T. Baba, "10 Gb/s operation of photonic crystal silicon optical modulators," Opt. Express **19**(14), 13000–13007 (2011).
26. Q. Xu, B. Schmidt, S. Pradhan, and M. Lipson, "Micrometre-scale silicon electro-optic modulator," Nature **435**(7040), 325–327 (2005).
27. X. Zheng, Y. Luo, J. Lexau, J. Liu, F. Guoliang Li, H. D. Thacker, I. Shubin, J. Yao, R. Ho, J. E. Cunningham, and A. V. Krishnamoorthy, "2-pJ/bit (On-Chip) 10-Gb/s digital CMOS silicon photonic link," IEEE Photon. Technol. Lett. **24**, 1260–1262 (2012).
28. Q. Fang, T.-Y. Liow, J. F. Song, K. W. Ang, M. B. Yu, G. Q. Lo, and D.-L. Kwong, "WDM multi-channel silicon photonic receiver with 320 Gbps data transmission capability," Opt. Express **18**(5), 5106–5113 (2010).
29. D. A. B. Miller, "Energy consumption in optical modulators for interconnects," Opt. Express **20**(S2 Suppl 2), A293–A308 (2012).
30. W. Bogaerts, S. K. Selvaraja, P. Dumon, J. Brouckaert, K. De Vos, D. Van Thourhout, and R. Baets, "Silicon-on-insulator spectral filters fabricated with CMOS technology," IEEE J. Sel. Top. Quantum Electron. **16**(1), 33–44 (2010).
31. W. A. Zortman, A. L. Lentine, D. C. Trotter, and M. R. Watts, "Low-voltage differentially-signaled modulators," Opt. Express **19**(27), 26017–26026 (2011).
32. K. Debnath, L. O'Faolain, F. Y. Gardes, D. Thomson, G. Reed, and T. F. Krauss, "Low insertion loss modulator based on a vertically coupled photonic crystal resonator," Proc. Soc. Photo Opt. Instrum. Eng. **8267**, 826701 (2011) (SPIE).
33. B. Huettl, R. Kaiser, W. Rehbein, H. Stolpe, Ch. Kindel, S. Fidorra, A. Steffan, A. Umbachl, and H. Heidrich, "Low noise monolithic 40 GHz mode-locked DBR lasers based on GaInAsP/InP," International Conference on Indium Phosphide and Related Materials, 633–636 (2005).
34. N. Sherwood-Droz and M. Lipson, "Scalable 3D dense integration of photonics on bulk silicon," Opt. Express **19**(18), 17758–17765 (2011).
35. A. Biberman, K. Preston, G. Hendry, N. Sherwood-Droz, J. Chan, J. S. Levy, M. Lipson, and K. Bergman, "Photonic network-on-chip architectures using multilayer deposited silicon materials for high-performance chip multiprocessors," J. Emerg. Technol. Comput. Syst. **7**(2), 7:1–7, 25 (2011).

1. Introduction

To reach the data transfer rates required for on- and off- chip interconnects, energy efficient Wavelength Division Multiplexing (WDM) is a key technique. Two major approaches may be identified in the literature, using either cascaded ring resonators [1] or arrayed waveguide gratings with broadband modulators [2, 3]. Ultimately, both of these approaches are limited by the free spectral range of the wavelength selective component. We now present a third approach, based on single mode Photonic Crystal (PhC) nanocavities, that provides a

#176485 - $15.00 USD Received 18 Sep 2012; revised 10 Nov 2012; accepted 14 Nov 2012; published 26 Nov 2012

significant increase in the number of available channels, thus providing a route to terabit/s on-chip links.

The attraction of PhC based cavities lies in their ability to strongly confine light in both space and time [4]. This provides compact devices with high Q-factors and enhanced light matter interaction. Many types of PhC cavities have already been reported that combine high Q-factor with ultra-low mode volume [5–7]. Due to the ultra-low mode volume, PhC cavities can be modulated with a power consumption of one to two orders of magnitude lower than conventional ring resonators. Along with this low power operation, PhC cavities eliminate the restriction on channel scalability, as the free spectral range can be very large (>100 nm) [6, 8]. Tanabe et al [9] have already exploited this advantage and demonstrated a PhC based electro-optic modulator on silicon, where two PhC waveguides are coupled by a PhC cavity and the transmission is modulated by carrier injection. Our novel architecture uses such a modulator as a building block and combines multiple devices into a WDM system via a vertically coupled bus waveguide.

Multiwavelength light sources have been highlighted as key components in such WDM networks [10] as they avoid the prohibitive power consumption entailed by banks of individual lasers. As calculated in [10], a 1-2W laser can potentially run a terascale network. Advances in multiwavelength lasers are putting such numbers within reach [11]. A centrally located, amplified comb laser provides such an option, with the added advantage that the light source heat dissipation is kept off the computing chip [12]. To demonstrate the full potential of our architecture, we use 5 cascaded PhC cavities to modulate 5 of the channels provided by a quantum dash comb laser.

2. Design

The basic layout is shown in Fig. 1(a). Light is first coupled from a lensed fiber into the dielectric bus waveguide made of silicon nitride (1.5μm wide and 500nm high) which runs directly above the photonic crystal cavities. This is reasonably well matched to a lensed fiber allowing us to achieve coupling losses of 3dB/facet in this experiment. Using techniques such as that employed in [13] or large mode area waveguides [14, 15], sub-dB insertion losses are possible with this approach.

When the wavelength of the incident light matches the resonance wavelength of the cavity, light couples efficiently into the cavity resulting in a reduction in transmission of the order of 10dB. By modifying the refractive index of the cavity, a strong modulation of the transmission can then be achieved. Figure 1(b) shows the cross section of the device where the cavity is embedded into a pin diode. Under forward bias, the excess carrier concentration in the intrinsic region provides a refractive change sufficient for intensity modulation of the waveguide output.

It is far from obvious that such efficient coupling between a low-index ($n\approx1.5$-1.9) dielectric waveguide and the high index ($n\approx3.5$) silicon layer is possible and represents one of the major innovations of this work. In standard directional coupler waveguides, a high coupling efficiency can only be achieved if the two waveguides are of the same size and of the same refractive index. Generally speaking, however, for efficient coupling of two modes, two conditions must be satisfied- a spatial mode overlap must exist and the two modes must be phase matched. In our case, the first condition can easily be satisfied by optimizing the physical gap between the waveguide and the cavity. Our geometry can also meet the second condition and achieve phase matching. The key lies in the small mode volume of the PhC cavity. As the mode volume decreases, the corresponding k-vector distribution expands- an initial obstacle to the creation of high Q-factor PhC cavities - and the problem of coupling reduces to that of matching the k-vector of the waveguide mode to that of a portion of the resonator. With a suitably designed PhC cavity, a low effective index mode may thus be matched to that of a silicon based resonator. The extinction ratio can then be controlled by optimizing the physical gap between the waveguide and the cavity and by fine-tuning the propagation constant of the waveguide with respect to the k-space distribution of the cavity. Figure 1(c) shows the Fourier space distribution of the resonant mode of the PhC cavity used

#176485 - $15.00 USD Received 18 Sep 2012; revised 10 Nov 2012; accepted 14 Nov 2012; published 26 Nov 2012

in this experiment. The structure of the cavity is shown in Fig. 2(a). The white circle represents the light cone and the yellow ellipse represents the position of the Fourier components of the silicon nitride waveguide at the resonance wavelength of the PhC cavity. The coupling between the waveguide mode and PhC cavity mode can then be controlled by optimizing the overlap between the two Fourier spaces. This is a versatile approach and with appropriate choice of waveguide effective index, coupling may be achieved to most PhC designs [5, 6].

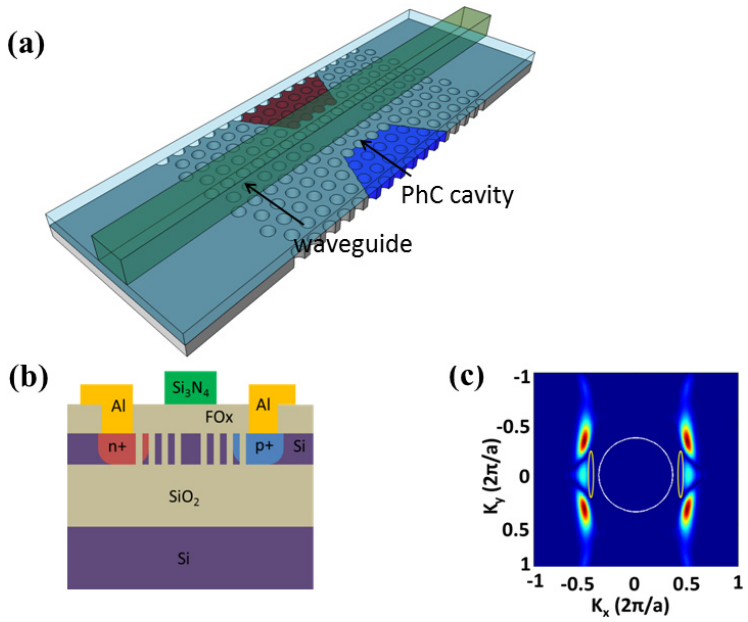

Fig. 1. (a) Schematic of the device, where the PhC cavity and the bus waveguide are vertically coupled through a buffer layer. An L3 PhC cavity is shown in the schematic for illustration purposes. The design of [7] is used experimentally; (b) Cross section of the device, consisting of a pin diode is embedded into a PhC cavity; (c) Fourier space distribution of the PhC cavity, the white circle representing the light cone and the yellow ellipses indicating the positions of the Fourier components of the silicon nitride waveguide mode.

2. Fabrication

Here we used the PhC cavity design introduced in [7] and realized a five channel WDM modulator circuit by cascading five PhC cavities that are designed to address successive wavelength channels. To create the pin junctions, five sets of doping windows were defined with "fingers" extending into the PhC regions, similar to [9], and doped using ion implantation of boron and phosphorous (~10^{19} cm^{-3}). The gap between the p and n regions is approximately 2μm. Even though the doping creates free-carrier losses, we have already established that Q-factors of 40,000 can be achieved with carrier densities of 10^{18} cm^{-3} in the center of the cavity [16], hence a doping density of 10^{19} cm^{-3} at this distance from the cavity center is not detrimental to the operation of the device.

#176485 - $15.00 USD Received 18 Sep 2012; revised 10 Nov 2012; accepted 14 Nov 2012; published 26 Nov 2012

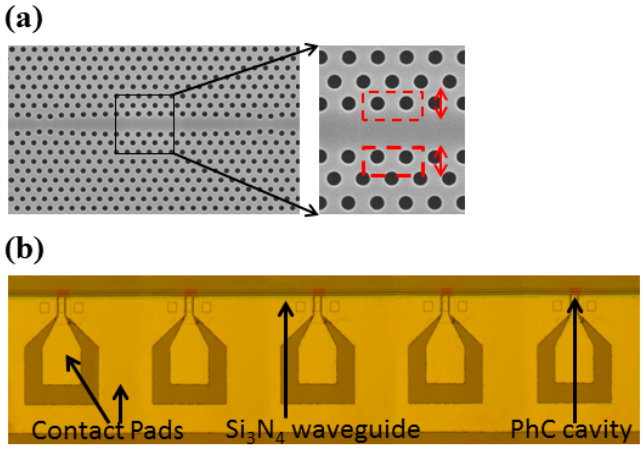

Fig. 2. (a) SEM image of the PhC cavity. All the five cavity designs were identical, except the positions of the four innermost holes of each cavity were tuned to achieve the required resonance wavelength, (b) top view of the cascaded PhC cavity based modulator set, where five cavities are coupled to a single silicon nitride waveguide.

Using electron beam lithography, the PhC designs are defined in the ZEP-520A layer and the pattern is transferred into the silicon layer by reactive ion etching with a SF_6/CHF_3 gas mixture, as described in more detail in [17]. To achieve different resonance wavelengths for each modulator, the positions of the four innermost holes of the cavities were tuned, as highlighted in Fig. 2(a). The entire device is then covered with spin-on-glass (FOx-14, Dow Corning). Although this process reduces the index contrast, it improves the CMOS compatibility of the final device [18], increases heat transport and allows us to control the coupling coefficient to the dielectric bus waveguide. The oxide layer thickness is then reduced to 200nm by RIE with CHF_3 gas, which is found to be the optimum thickness for efficient coupling while maintaining a high Q. A 500nm thick layer of silicon nitride is then deposited using Plasma Enhanced Chemical Vapor Deposition and the waveguide is defined on top of all the cavities as shown in Fig. 2(b). The dimensions of the silicon nitride waveguide are 1.5μm × 500nm, which is large enough to support higher order modes. In the measurement, however, only the fundamental mode tends to get excited, which is evident from the relatively large extinction ratio that we observe. Furthermore only the fundamental waveguide mode will be k-vector matched to the cavity mode. After defining the waveguide, electrical contacts are created by etching via holes through the nitride and oxide layers and depositing aluminum contacts by thermal evaporation. The metal-semiconductor contact was ohmic, though with a relatively high resistance.

3. Electro-optic modulation

The transmission spectrum of the fabricated device was first characterized with a tunable laser end-fire coupled into the bus waveguide. Figure 3(a) shows the normalized transmission spectrum of the device, with each of the five transmission dips corresponding to one of the five cavities. The loaded quality factor of the cavities is around 15,000, which corresponds to an unloaded quality factor of 70,000. Since the ultimate limit on the modulation speed is given by the photon life time in the cavity, we designed the cavities to be limited to Q≈15,000 by the coupling coefficient; for a Q-factor of 15,000, the photon lifetime is ≈12 ps and the modulation limit is 10s of GHz. The extinction ratio depends on the coupling coefficient between the cavity and the waveguide, and was designed to be 10 dB or above to reach the target Bit error rates [19]. For the as-fabricated device, the five channels are not quite equally spaced [20]; we note that these channel spacing values can be further improved by trimming techniques such as laser assisted local oxidation [21], or by using highly efficient active tuning with integrated heaters [22].

#176485 - $15.00 USD Received 18 Sep 2012; revised 10 Nov 2012; accepted 14 Nov 2012; published 26 Nov 2012

In order to test the high speed electro-optic modulation properties of the device, a PRBS unit, generating 127 bit long sequence, was used to drive the PhC cavities electrically and the electrical signal was applied to the devices via a high speed RF probe. An additional DC bias was added via a bias T. The peak-to-peak voltage of the driving signal was 700mV and the DC bias was set to + 4V. Figure 3(b) and 3(c) shows the eye diagrams of the modulated optical output at 0.5Gbit/s and at 1Gbit/s, respectively for the second modulator. The operating wavelength was chosen to be the resonance wavelength (1549.5nm) of the second modulator at 4V forward bias.

The AC component of the power consumption was calculated as $P_{ac} = V_{rms}^2/R$, giving a value of 0.625μW, or ~0.6fJ/bit at 1Gbit/s modulation (assuming a sinusoidal waveform). The energy consumed as a result of the DC bias was 38μW (38fJ/bit for 1Gbit/s operation). We note that such a large DC bias was required because of the high resistance (~100 KΩ) of our current device.

To estimate the switching energy required for a transition from the OFF to ON state, a more fundamental indication of the device performance, we followed the method used in [23]. For an input voltage swing of 700mV, the extinction ratio was 3.5dB at 1Gbit/s, which corresponds to a resonance wavelength shift of 20 pm and a refractive index change in the silicon device layer of $\Delta n = 4.48 \times 10^{-5}$. This refractive index change corresponds to a carrier density change of $\Delta N = 6.7 \times 10^{15}$ cm^{-3} in the intrinsic region of the modulator. Given the physical volume of the intrinsic region of 2.2 μm^3, the switching energy for our device is therefore approximately 1.6 fJ, which is amongst the lowest ever reported.

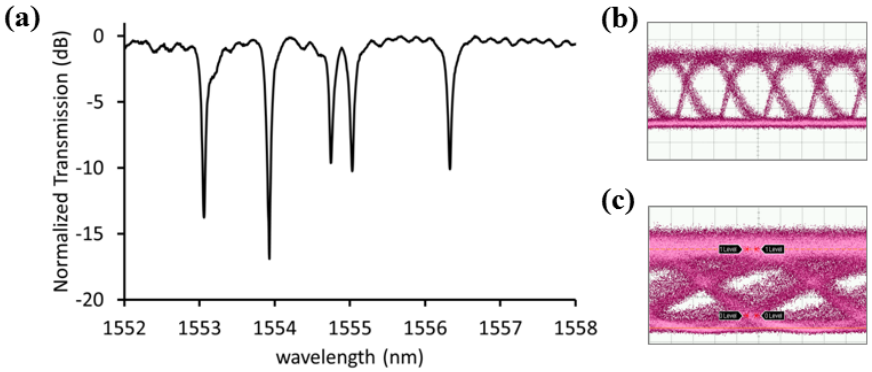

Fig. 3. (a) Normalized transmission spectrum (TE input polarization) of the silicon nitride waveguide vertically coupled to five PhC cavities. The dips correspond to each cavity mode, (b), (c) eye diagrams of the modulated optical output of the first modulator at 0.5Gbit/s and 1.0Gbit/s respectively. The horizontal-axis scale is 1ns/division for 0.5gbit/s and 200ps/div for 1 Gbit/s. In this case, the number of channels is limited by the 8nm FSR of the multimode cavity used here. This is not a fundamental limit and this coupling approach may be extended to cavities with very large FSR's such as [5, 6].

4. Multiplexing

To observe multiplexing, we applied the driving signal successively to each modulator and recorded the optical output at the resonance wavelength of each individual modulator. Figure 4 shows the eye diagrams of the five channels, each operating at 0.5 Gbit/s. To improve the extinction ratio further, the peak-to-peak voltage of the driving signal was set to 1.7 V. This resulted in an extinction ratio of more than 7dB for each channel. Here, we used carrier injection for the initial demonstration of modulation and as a result the speed is limited by the free carrier lifetime in the intrinsic region of the pin diode. This is not a fundamental limit, however, as depletion-type modulation, for example, can easily achieve the carrier density change of 5×10^{15} cm^{-3} required for a 3dB extinction ratio. Modulation speeds up to 50 Gbit/s have already been demonstrated with this technique [24] and have also been shown to be compatible with PhC designs [25]. Due to the small device area, fF capacitances can be

#176485 - $15.00 USD Received 18 Sep 2012; revised 10 Nov 2012; accepted 14 Nov 2012; published 26 Nov 2012

realized in this configuration. For operation in carrier depletion mode, the power consumption is determined only by the switching energy and from the earlier numbers, values of 0.4fJ/bit could be expected (as the 0-1 transitions have a 0.25 probability of occurring).

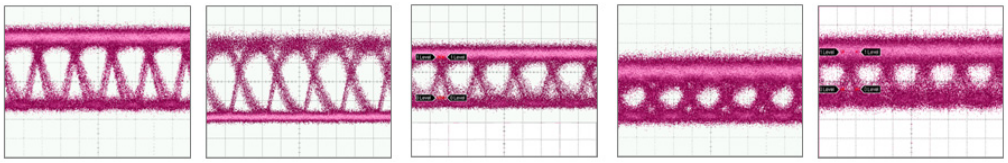

Fig. 4. Eye diagrams at 0.5Gbit/s for channels 1-5. Open eyes were observed for each channel. The horizontal-axis scale is 1ns/division

Due to their large Free Spectral Range (FSR) [4], it is straightforward to fabricate large arrays of single mode PhC cavities. The width of the photonic bandgap (300-400nm) is the ultimate limit making this technique very scalable. This scalability, combined with the low switching energy, the small footprint and the low insertion loss makes our architecture very suitable for dense WDM operation and has the potential for Tbit/s data transmission. Even with the low modulation speeds reported here, such a FSR could support the 1000 channels required for a Tbit/s data transmission with dramatically lower area and power consumption than other approaches. Increasing the modulation speed to a reasonable 10Gbit/s reduces the channel number to very practical numbers.

Table 1. Comparison of Different Low Power WDM Modulator Techniques

Type	Channel spacing (nm)	FSR (nm)	Area/ channel (μm^2)*	Maximum channels	Excess loss (dB)**	Switching Energy (fJ)
Rings	0.6 [1]	18 [1], 19 [19]	400	30	9 [26], 11 [27]	55 [23]
SiN AWG [2]	0.8	12.8	300k	16	14	Ge EA modulator 3 [29]
Si AWG [28]	0.8	74	12k	46	10	
Echelle [30]	3	90	16.6k	30	16	
Microdisks [31]	-	-	25	-	10	12
This approach	0.44	100 + [4]	100	220 +	6 (2.8 [32])	1.6

For the channel numbers and spacings, in order to show the full potential of the various systems the best case numbers are taken from the respective papers. Microdisk modulators are a powerful option, intermediate between the ring resonators and PhC resonators in terms of mode volume and FSR. However, to our knowledge, cascadeability has not yet been demonstrated.

*This is the area of each resonant component (with an allowance for trenches etc) or the total device area divided by the number of channels.

**Defined here as the sum of the coupling loss and the loss in the demux/mux elements. Losses in the modulator are generally in 3-5dB range [27], but strongly depend on the extinction ratio and energy/bit values used thus making a comparison based on this number difficult. NB For the non-resonant approaches, this loss is calculated assuming both a demultiplexing and multiplexing element. Losses in interfacing between the demux/mux and the modulators are also ignored in this case.

In Table 1, we make a comparison with other results in the literature. There are two categories- resonant and non-resonant approaches. There is a large number of options for non-resonant modulators; here, we limit ourselves to the most energy efficient, namely waveguide integrated Germanium electroabsorption modulators (at 0.75fJ/bit) [29]. Such relatively broadband modulator may be combined with a range of demultiplexing/multiplexing elements.

In resonator approaches, the number of channels scales with the finesse of the resonator ($FSR/\Delta\lambda$). For an arrayed waveguide grating, the channel number is given by the number of waveguides. The channel spacings are then given by the resonator Q-factor and the interference order of the arrayed waveguide grating respectively. These considerations place

#176485 - $15.00 USD Received 18 Sep 2012; revised 10 Nov 2012; accepted 14 Nov 2012; published 26 Nov 2012

limitations on the area and channel number of the various approaches and are clearly illustrated in the table. By virtue of its high FSR, the PhC cavity provides the greatest number of channels making it one of the most promising routes to high bandwidth links. It should be noted that temperature and disorder stability is another key issue, with the Silicon Nitride AWG of [2] one of the best solutions in this regard.

To demonstrate the full potential of our approach, we used a multi-wavelength comb laser [33] source with a spacing of 50 GHz (0.44nm) between each channel, shown in the inset of Fig. 5. The resonance wavelength of each of the five cavities was actively tuned by adjusting the DC bias, which has the effect of thermo-optically tuning the resonances to match five consecutive lines of the comb laser as shown in Fig. 5(a). Figure 5(b) shows the output spectrum of the waveguide when none of the cavity wavelengths are aligned with the lines of the laser (each spike was normalized to unity for clarity) and Fig. 5(c) shows the same spectrum when the cavities are aligned to the lines of the comb laser. This clearly demonstrates the scalability and multi-wavelength operation of our architecture.

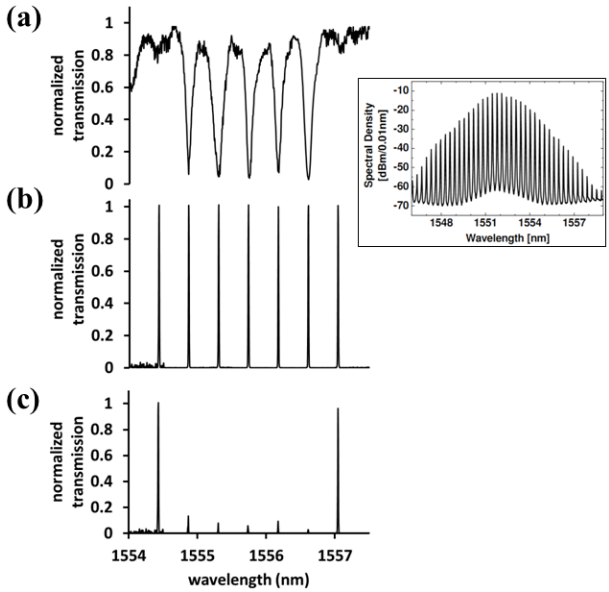

Fig. 5. Normalized transmission spectrum of the bus waveguide with a tunable laser when each cavity is actively tuned to match the comb laser spectrum, (b) normalized transmission spectrum of the bus waveguide with the comb laser when cavity resonances are not aligned with the comb laser spectrum, (c) normalized transmission spectrum of the bus waveguide with the comb laser when cavity resonances are aligned with the comb laser, inset shows the comb laser spectrum

4. Conclusion

We have demonstrated a compact cascaded modulator architecture based on PhC nanocavities connected by a dielectric bus waveguide. The key feature of the architecture is the efficient coupling between the low index bus waveguide and the high index silicon PhC cavities, enabled by careful k-vector matching. We demonstrated how an array of such cavities can be operated with a single source, i.e. a comb laser, to achieve on-chip WDM operation, one of the first demonstrations of this kind. The switching energy (Off-On state) was only 1.6 fJ, one of the lowest yet reported for a silicon electro-optic modulator. The k-space matching technique allows effortless transfer of light from low refractive index passive components into the high index active layers. The attraction of deposited layers, such the Silicon Nitride used here, for on-chip networks has already been highlighted [34, 35], as the low loss and relatively tight bending radii makes such waveguides ideal for the realization of complex

#176485 - $15.00 USD Received 18 Sep 2012; revised 10 Nov 2012; accepted 14 Nov 2012; published 26 Nov 2012

passive on-chip networks. Our technique solves the problematic interfacing between the active (silicon) and passive (silicon nitride) components allowing the full potential of on-chip networks to be realized. Additionally, the potentially sub-dB insertion losses of these waveguides are ideal for the off-chip connections. Finally, by removing the bus waveguide from the active device layer and placing it above, the area available for electronic circuitry is maximized, while keeping the active photonics in crystalline silicon- a further advantage for front-end CMOS integration. Ultimately, the key advantages of our approach derive from the high finesse of the photonic crystal cavity. Only a high finesse cavity can combine small size, therefore low capacitance, with narrow bandwidth and large free spectral range, which singles out the photonic crystal approach as uniquely advantageous.

Acknowledgment

This work was funded by the EPSRC in the UK under the UK Silicon Photonics project. Liam O'Faolain also acknowledges support from an SU2P fellowship (www.SU2P.com). The authors are grateful to Dr. Kieran Deasy of Sheffield University for depositing Silicon Nitride. The authors would also like to thank Dr. Karl Welna and Dr. Marcello Ferrera for helping with device fabrication and acknowledge David A. B Miller for useful discussions.

#176485 - $15.00 USD Received 18 Sep 2012; revised 10 Nov 2012; accepted 14 Nov 2012; published 26 Nov 2012